Theory and modelling of constant-Q *P*- and *S*-waves using fractional spatial derivatives

Tieyuan Zhu[1] and José M. Carcione[2]

[1]*Department of Geophysics, Stanford University, Stanford, CA 94305, USA. E-mail: tieyuanzhu@gmail.com*
[2]*Istituto Nazionale di Oceanografia e di Geofisica Sperimentale (OGS), Borgo Grotta Gigante* 42c, *I-34010 Sgonico, Trieste, Italy*

SUMMARY

We derive a time-domain differential equation for modelling seismic wave propagation in constant-*Q* viscoelastic media based on fractional spatial derivatives, specifically Laplacian differential operators of fractional order. The stress–strain relation is derived from the classical equation expressed in terms of fractional time derivatives. The new formulation has the advantage of not requiring additional field variables that increase the computer time and storage significantly. The spatial derivatives are calculated with a generalization of the Fourier pseudospectral method to the fractional-derivative case. The accuracy of the numerical solution is verified against an analytical solution in a homogeneous medium. An example shows that the proposed wave equation describes the constant-*Q* attenuation and velocity dispersion behaviour observed in Pierre Shale. Finally, we consider a plane-layer model and the Marmousi model to show how the new formulation applies to inhomogeneous media.

Key words: Numerical solutions; Seismic attenuation; Computational seismology; Wave propagation.

1 INTRODUCTION

Seismic wave propagation has anelastic characteristics in real Earth materials. Particularly, in exploration geophysics the target area (the hydrocarbon reservoir) shows high seismic attenuation (i.e. low quality factor, *Q*) which may be caused by the presence of overpressured free gas accumulations (e.g. Carcione *et al.* 2003; Dvorkin & Mavko 2006). As a result, the recorded signals are significantly affected in amplitude and phase. Therefore, an accurate wavefield modelling approach should be able to account for the effects of attenuation and velocity dispersion.

One of the first attempts to model anelastic wave propagation was carried out by Carcione *et al.* (1988), based on the generalized Zener model and memory variables. This model uses a spectrum of relaxation mechanisms to describe the constitutive relation. It involves a set of first-order differential equations that can be solved with numerical methods. This approach has been widely applied in geophysical studies (Carcione 1990; Robertsson *et al.* 1994; Xu & McMechan 1995; Hestholm 1999; Komatitsch *et al.* 2004; Zhu *et al.* 2013).

An alternative approach for modelling constant-*Q* given by Kjartansson (1979) is more attractive because it requires three parameters, namely, *Q,* a reference phase velocity and a reference frequency. This model has been shown to describe the behaviour of seismic waves in Pierre shale (McDonal *et al.* 1958; Carcione *et al.* 2002). The model involves a fractional time derivative, that is an irrational (or non-integer) degree of the time derivative (Caputo & Mainardi 1971). The Grünwald-Letnikov approximation (Podlubny

1999) is used to compute this time derivative (Carcione *et al.* 2002; Carcione 2009). However, this formulation is based on the history of the wavefield, thus requiring to store in memory all the previous values to present time. It becomes unaffordable for practical seismic modelling studies, in particular for 3-D simulations, even though it is possible to truncate the fractional operator after a given time period (Podlubny 1999; Carcione *et al.* 2002).

To avoid the memory requirements of the fractional time operators, we have developed a constant-*Q* wave equation using fractional Laplacian operators (Carcione 2010; Treeby & Cox 2010). Zhu & Harris (2013) presented the viscoacoustic case, that is only *P*-wave propagation. Here, we consider the viscoelastic case, that is propagation of *P* and *S* waves. We transform the fractional time derivative to a fractional Laplacian operator (Chen & Holm 2004; Carcione 2010). This operation, computed with the fractional Fourier pseudospectral method, avoids the storage of wavefields, rendering the modelling as efficient as the simulation in lossless media.

The paper is organized as follows: First, we review the derivation of the viscoacoustic stress–strain relation using the fractional Laplacian operator. Then, we derive the viscoelastic constitutive equation from the formulation given in Carcione (2009). The novel stress–strain relation has two sets of fractional Laplacian operators, one for *P* waves and another for *S* waves. The modelling algorithm is based on the method introduced by Carcione (2010), where the spatial derivatives are computed by a generalization of the Fourier pseudospectral method to the fractional case. Finally, we validate the modelling algorithm with an analytical solution for a 2-D

homogeneous medium and further illustrate the method with two seismic applications in inhomogeneous media.

2 THEORY

2.1 Fractional viscoacoustic wave equation

We consider the following phenomenological constitutive relation based on the fractional time derivative (Caputo 1967; Carcione *et al.* 2002) that defines the stress–strain relation in attenuating media

$$\sigma = \left(\frac{M_0}{t_0^{-2\gamma}}\right)\frac{\partial^{2\gamma}\varepsilon}{\partial t^{2\gamma}}, \tag{1}$$

where σ is the trace of the stress tensor, ε is the trace of the strain tensor, $M_0 = \rho c_0^2 \cos^2(\pi\gamma/2)$ is a bulk modulus, $t_0 = 1/\omega_0$ is a reference time, c_0 is a reference velocity, ρ is the mass density and $\gamma = (1/\pi)\tan^{-1}(1/Q)$ is the fractional order, satisfying $0 < \gamma < 0.5$ for any positive value of Q. ω_0 is an arbitrary reference frequency, which should be higher than the source frequencies to guarantee pulse delay with respect to the lossless case. The complete formulation of the constant-Q model can be found in Kjartansson (1979), Carcione *et al.* (2002) and Carcione (2009).

Next, we construct a phenomenological stress–strain relation based on fractional spatial differential operators. Applying a wavenumber-frequency domain Fourier transform to eq. (1) yields,

$$\hat{\sigma} = M_0 \omega_0^{-2\gamma}(i\omega)^{2\gamma}\hat{\varepsilon}, \tag{2}$$

where ω is the angular frequency and i is the imaginary number. Since $i^{2\gamma} = \cos(\pi\gamma) + i\sin(\pi\gamma)$, eq. (2) can be written as

$$\hat{\sigma} \approx M_0 c_0^{2\gamma} \omega_0^{-2\gamma} \cos(\pi\gamma) k^{2\gamma}\hat{\varepsilon} + (i\omega) M_0 c_0^{2\gamma-1}\omega_0^{-2\gamma}$$
$$\times \sin(\pi\gamma) k^{2\gamma-1}\hat{\varepsilon}, \tag{3}$$

where we have introduced the wavenumber $k = \omega/c_0$. The fractional Laplacian is defined in Chen & Holm (2004) as,

$$(-\nabla^2)^{\alpha/2}\sigma(\mathbf{r}, t) \overset{F}{\longleftrightarrow} k^\alpha \hat{\sigma}(k, \omega), \quad 0 < \alpha < 2. \tag{4}$$

Applying the inverse Fourier transform to eq. (3), we obtain

$$\sigma = M_0 c_0^{2\gamma}\omega_0^{-2\gamma}\cos(\pi\gamma)\left(-\nabla^2\right)^\gamma \varepsilon + M_0 c_0^{2\gamma-1}\omega_0^{-2\gamma}$$
$$\times \sin(\pi\gamma)\frac{\partial}{\partial t}\left(-\nabla^2\right)^{\gamma-1/2}\varepsilon. \tag{5}$$

Combining eq. (5) with the momentum-mass conservation equations, a first-order fractional wave equation can be obtained. Based on the plane-wave analysis of Appendix A, we verify that the phase velocity and quality factor are similar to those of the constant-Q model proposed by Kjartansson (1979) and Carcione *et al.* (2002). Wavefield simulations can be found in Zhu & Harris (2013).

2.2 Fractional viscoelastic wave equation

Similarly, we construct a viscoelastic stress–strain relation from the constitutive equation given by Carcione (2009),

$$\sigma_{ij} = C_\lambda D^{2\gamma_P}\varepsilon_{kk}\delta_{ij} + 2C_\mu D^{2\gamma_S}\left(\varepsilon_{ij} - \varepsilon_{kk}\delta_{ij}\right), \tag{6}$$

where δ_{ij} is the Kronecker delta, i, j, k are spatial indices and the fractional time-derivative operators for the P- and S-waves are defined as

$$D^{2\gamma_{P,S}} = \frac{\partial^{2\gamma_{P,S}}}{\partial t^{2\gamma_{P,S}}}. \tag{7}$$

Moreover,

$$C_\lambda = M_0\omega_0^{-2\gamma_P}, \quad C_\mu = \mu_0\omega_0^{-2\gamma_S}, \tag{8}$$

with μ_0 the shear modulus and

$$\gamma_{P,S} = \frac{1}{\pi}\tan^{-1}\left(\frac{1}{Q_{P,S}}\right), \tag{9}$$

where Q_P and Q_S are the P- and S-wave quality factors, respectively. Einstein's convention of repeated indices is assumed. According to the constant-Q model (Carcione 2009), the P-wave modulus M_0 and the S-wave modulus μ_0 are, respectively, given by

$$M_0 = \rho c_{P0}^2 \cos^2\left(\mathrm{atan}(Q_P^{-1})/2\right), \mu_0 = \rho c_{S0}^2 \cos^2\left(\mathrm{atan}(Q_S^{-1})/2\right), \tag{10}$$

where c_{P0} and c_{S0} are the P- and S-wave velocities at the reference frequency, respectively.

Consider the 2D case and the (x,z)-plane. We have

$$\sigma_{11} = C_\lambda D^{2\gamma_P}(\varepsilon_{11} + \varepsilon_{33}) - 2C_\mu D^{2\gamma_S}\varepsilon_{33}, \tag{11}$$

$$\sigma_{33} = C_\lambda D^{2\gamma_P}(\varepsilon_{11} + \varepsilon_{33}) - 2C_\mu D^{2\gamma_S}\varepsilon_{11}, \tag{12}$$

$$\sigma_{13} = 2C_\mu D^{2\gamma_S}\varepsilon_{13}. \tag{13}$$

Now, we perform a Fourier transform to the wavenumber-frequency domain and replace ω by $c_{P0}k$ in terms containing the $D^{2\gamma_P}$ derivative and by $c_{S0}k$ in terms containing the $D^{2\gamma_S}$ derivative. This *ad hoc* construction provides a stress–strain relation based on fractional spatial derivatives

$$\hat{\sigma}_{11} = C_\lambda c_{P0}^{2\gamma_P}\left[\cos(\pi\gamma_P) + i\sin(\pi\gamma_P)\right]k^{2\gamma_P}(\hat{\varepsilon}_{11} + \hat{\varepsilon}_{33})$$
$$- 2C_\mu\left[\cos(\pi\gamma_S) + i\sin(\pi\gamma_S)\right]c_{S0}^{2\gamma_S}k^{2\gamma_S}\hat{\varepsilon}_{33}. \tag{14}$$

Applying inverse Fourier transforms yields

$$\sigma_{11} = C_\lambda c_{P0}^{2\gamma_P}\Big[\cos(\pi\gamma_P)\left(-\nabla^2\right)^{\gamma_P}$$
$$+ c_{P0}^{-1}\sin(\pi\gamma_P)\frac{\partial}{\partial t}\left(-\nabla^2\right)^{\gamma_P-1/2}\Big](\varepsilon_{11} + \varepsilon_{33})$$
$$- 2C_\mu c_{S0}^{2\gamma_S}\Big[\cos(\pi\gamma_S)\left(-\nabla^2\right)^{\gamma_S}$$
$$+ c_{S0}^{-1}\sin(\pi\gamma_S)\frac{\partial}{\partial t}\left(-\nabla^2\right)^{\gamma_S-1/2}\Big]\varepsilon_{33}, \tag{15}$$

which can be re-written as

$$\sigma_{11} = \left[\tau_P\frac{\partial}{\partial t}\left(-\nabla^2\right)^{\gamma_P-1/2} + \eta_P\left(-\nabla^2\right)^{\gamma_P}\right](\varepsilon_{11} + \varepsilon_{33})$$
$$- 2\left[\tau_S\frac{\partial}{\partial t}\left(-\nabla^2\right)^{\gamma_S-1/2} + \eta_S\left(-\nabla^2\right)^{\gamma_S}\right]\varepsilon_{33}, \tag{16}$$

where

$$\tau_P = C_\lambda c_{P0}^{2\gamma_P-1}\sin(\pi\gamma_P), \tag{17}$$

$$\eta_P = C_\lambda c_{P0}^{2\gamma_P}\cos(\pi\gamma_P), \tag{18}$$

$$\tau_S = C_\mu c_{S0}^{2\gamma_S-1}\sin(\pi\gamma_S), \tag{19}$$

$$\eta_S = C_\mu c_{S0}^{2\gamma_S}\cos(\pi\gamma_S). \tag{20}$$

Similarly, eqs (12) and (13) become

$$\sigma_{33} = \left[\tau_P \frac{\partial}{\partial t} \left(-\nabla^2 \right)^{\gamma_P - 1/2} + \eta_P \left(-\nabla^2 \right)^{\gamma_P} \right] (\varepsilon_{11} + \varepsilon_{33})$$
$$- 2 \left[\tau_S \frac{\partial}{\partial t} \left(-\nabla^2 \right)^{\gamma_S - 1/2} + \eta_S \left(-\nabla^2 \right)^{\gamma_S} \right] \varepsilon_{11}, \qquad (21)$$

$$\sigma_{13} = 2\tau_S \frac{\partial}{\partial t} \left(-\nabla^2 \right)^{\gamma_S - 1/2} \varepsilon_{13} + 2\eta_S \left(-\nabla^2 \right)^{\gamma_S} \varepsilon_{13}, \qquad (22)$$

respectively. Combining eqs (16), (21) and (22) with the momentum conversation equations, we obtain the fractional viscoelastic wave equation. The complete first-order velocity-stress equations are given in Appendix B. When $Q_{P,S} \rightarrow \infty$ ($\gamma_{P,S} \rightarrow 0$), we obtain the elastic case.

Anelastic propagation described by viscoelasticity is a phenomenological model, whose prediction properties depend on a number of parameters, which are reduced to a minimum in this formulation. The fact that the parameters are assumed to be constant in the derivation of the fractional viscoelastic wave equation does not preclude the fact to use the modelling method to simulate real seismic data for an arbitrary heterogeneous model of the Earth. The essential fact is that this *ad hoc* construction of the rheological equations allows us to avoid the time convolutions and therefore to save substantial computer time.

To solve the wave equation in inhomogeneous media, we use the numerical approach given in Carcione (2010). We calculate the first-order spatial derivatives with the staggered-grid pseudospectral method that minimizes spatial numerical dispersion and nonphysical ringing (Özdenvar & McMechan 1996; Carcione 1999). The fractional Laplacian operators are implemented with the fractional Fourier pseudospectral method as shown by Carcione (2010). The perfectly matched layer (PML) approach is used as absorbing boundary to remove non-physical events from the sides of the mesh (e.g. Berenger 1994; Carcione & Kosloff 2013).

3 NUMERICAL EXAMPLES

We validate the proposed viscoelastic wave equation with experimental data and the numerical solver by comparison to the analytical solution. McDonal *et al.* (1958) reported seismic data from Pierre shale in Colorado which present an approximate constant-Q behaviour, with attenuation coefficients $\alpha_p = 0.12 f$ dB/kft and $\alpha_s = 1.05 f$ dB/kft, where f is the frequency. The *P*- and *S*-wave quality factors of Pierre shale are $Q_P = 32$ and $Q_S = 10$, and the respective velocities are 2164 and 802 m s^{-1} at the reference frequency of 100 Hz (Carcione 2009). We assume a shale density of 2.2 g cm^{-3}. The simulations are performed with a 612×612 mesh, 1-m grid spacing along the *x*- and *z*-directions and a time step of 9.24×10^{-5} s. A Ricker wavelet source with 100 Hz centre frequency is located at (300, 300) m and two receivers at (360, 360) m and (380, 380) m. Fig. 1 shows the recorded waveforms. Then, the attenuation coefficient α (in dB/km) and the phase velocity are calculated with the amplitude spectral ratio as (Picotti & Carcione 2006; Treeby & Cox 2010)

$$\alpha(\omega) = -20 \log_{10} \left(\frac{A_2}{A_1} \right) \Big/ d, \qquad (23)$$

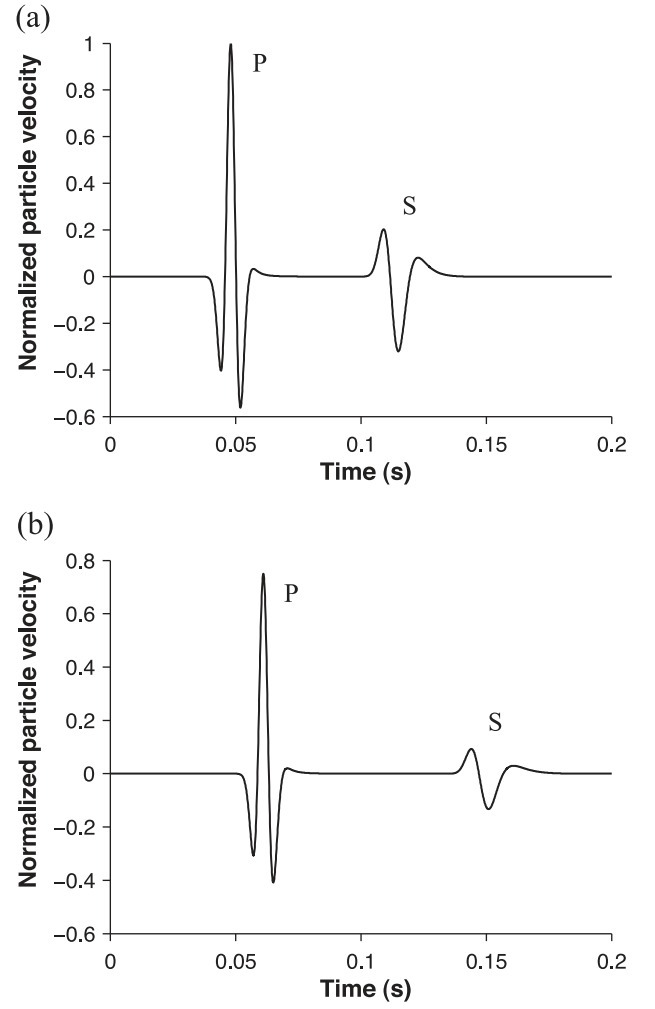$$c(\omega) = \frac{\omega d}{\phi_1 - \phi_2}, \qquad (24)$$

Figure 1. Normalized waveforms recorded at receivers located at (360, 360) m (a) and (380, 380) m (b). The amplitude differences are caused by geometric spreading and intrinsic attenuation.

respectively, where $A_{1,2}$ are the amplitude spectra at the two receivers, $\phi_{1,2}$ are the phases and d is the propagation distance in meters.

Fig. 2 displays the calculated attenuation factor (circles), the theoretical curves (solid lines) and the experimental results (triangles) from McDonal *et al.* (1958). Figs 3(a) and (b) illustrate the *P*- and *S*-wave phase velocity dispersion in Pierre shale. Overall, the calculated attenuation and dispersion values agree with the theoretical constant-Q curves as well as with the experimental results. We note that the calculated *S*-wave attenuation factor and phase velocity oscillate at high frequencies due to the strong attenuation. Similar observations were made by Wuenschel (1965) and Zhu & Harris (2013).

Next, we consider a homogeneous model, where the analytical solution is available, in order to verify the accuracy of the algorithm. For completeness, the Green's function is given in Appendix C [see also Carcione (2009)]. The *P*- and *S*-wave velocities are 2500 and 1500 m s^{-1}, respectively, and the density is 2200 kg m^{-3}. We have considered $Q_P = 32$ and $Q_S = 16$. The model is discretized in a mesh with 512×512 grid points using a 10-m grid spacing in both the horizontal and vertical directions, and the time step is
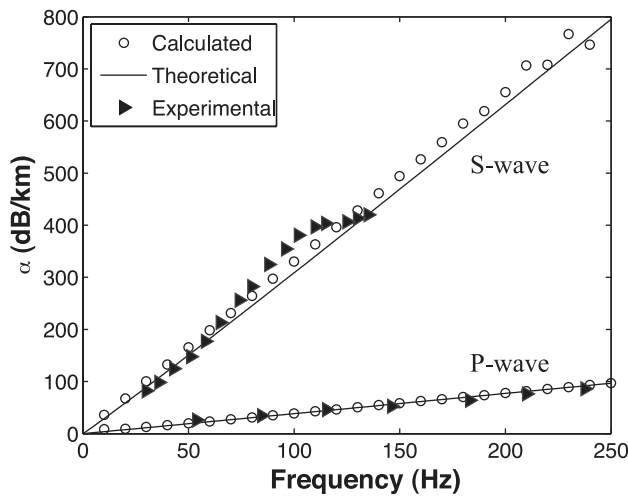
Figure 2. *P*- and *S*-wave attenuation coefficients. The solid lines represent the theoretical attenuation based on the constant-*Q* model. The dotted points are estimated from the waveforms in Fig. 1. The triangles correspond to the experimental data reported by McDonal *et al.* (1958).
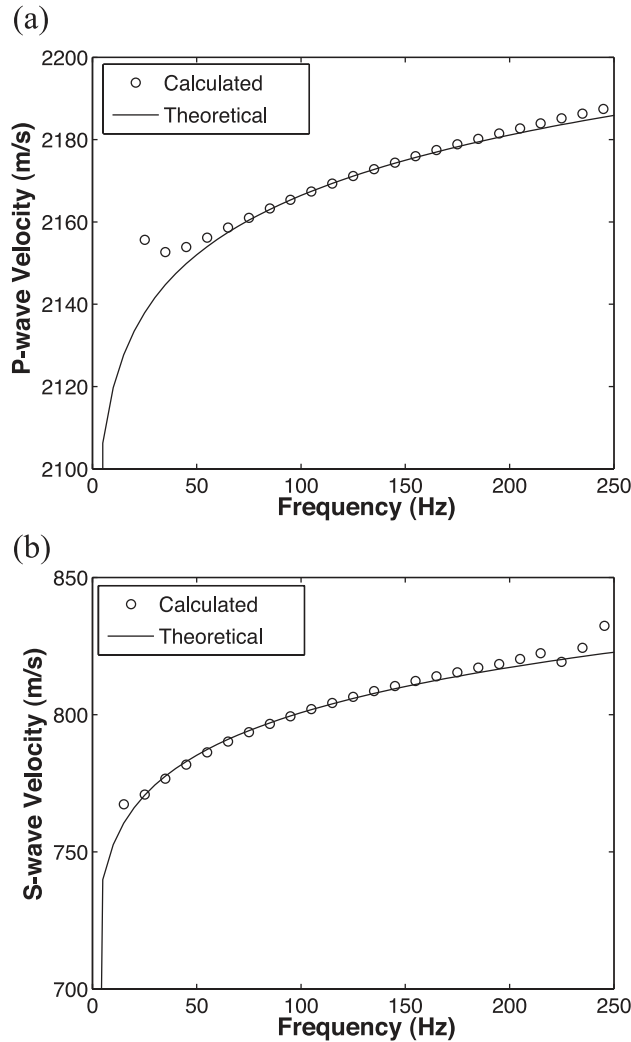

Figure 3. *P*-wave (a) and *S*-wave (b) phase velocity dispersion. The solid lines represent the theoretical phase velocity. The dotted points are estimated from the waveform in Fig. 1.
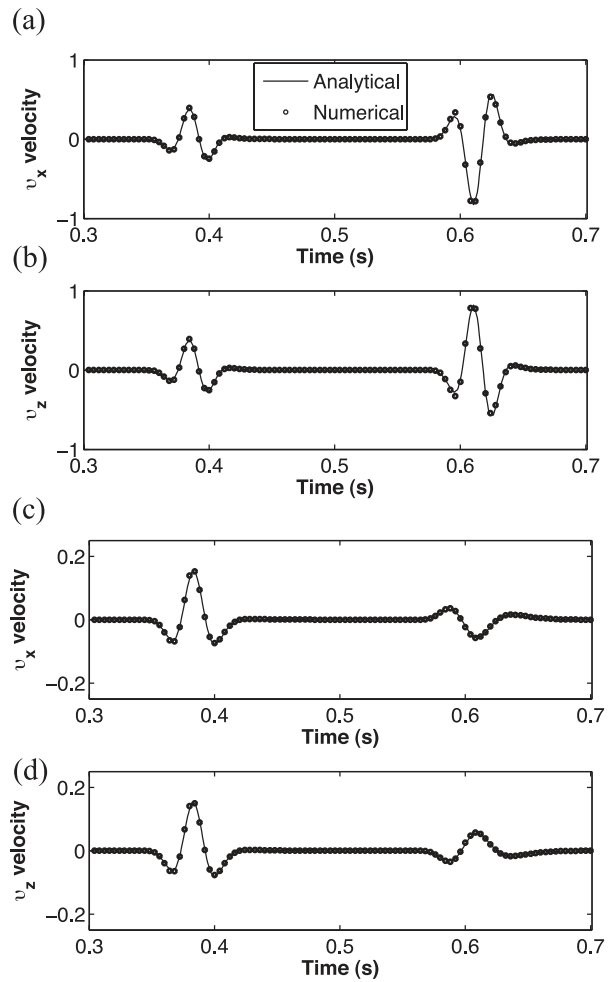

Figure 4. Comparison of the elastic and viscoelastic numerical results with the respective analytical solutions (normalized values). Elastic case: (a) horizontal υ_x and (b) vertical υ_z, where Q_p and Q_S take infinite values. Viscoelastic case: (c) horizontal υ_x and (d) vertical υ_z, where $Q_p = 32$ and $Q_S = 16$. A vertical source is located at (395, 395) m and the receiver position is (995, 995) m.

0.8 ms. The source (a vertical force) has a Ricker time history with 25 Hz centre frequency. Fig. 4 compares the numerical and analytical solutions. As can be seen, the two solutions agree very well.

In the third example, we consider seismic wave propagation in inhomogeneous media. The model shown in Fig. 5 consists of three layers. The low velocities and low Q_p of the middle layer simulate a high-attenuation reservoir. The medium is discretized with 462 × 206 grid points and uniform vertical and horizontal grid spacings of 10 m. The source is a vertical force with a Ricker-wavelet time history and a central frequency of 25 Hz (~5.55 grid points per shortest wavelength), located at (2310, 250) m. 246 receivers are located at a depth of 250 m ranging from 10 to 4510 m, with a spacing 20 m. The time step of the modelling algorithm is 0.5 ms. PML absorbing strips of width 20 grid points are implemented at the four boundaries of the computational mesh to avoid wraparound.

Fig. 6 shows the elastic and viscoelastic vertical-component snapshots at 0.5 s. The snapshots in Figs 6(a) and (b) clearly show the direct *P* wave and other events, for example, the reflected PP and
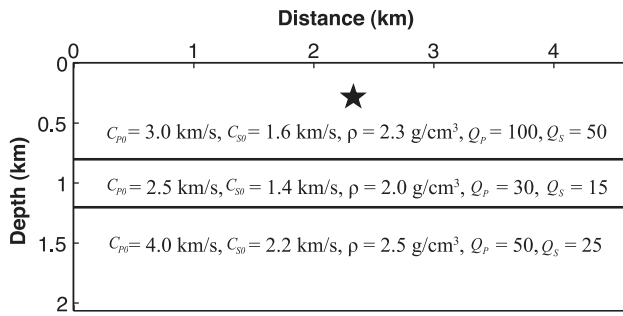
Figure 5. Layered model with the properties used in the calculation of the synthetic data. The black star represents the source location at (2310, 250) m.
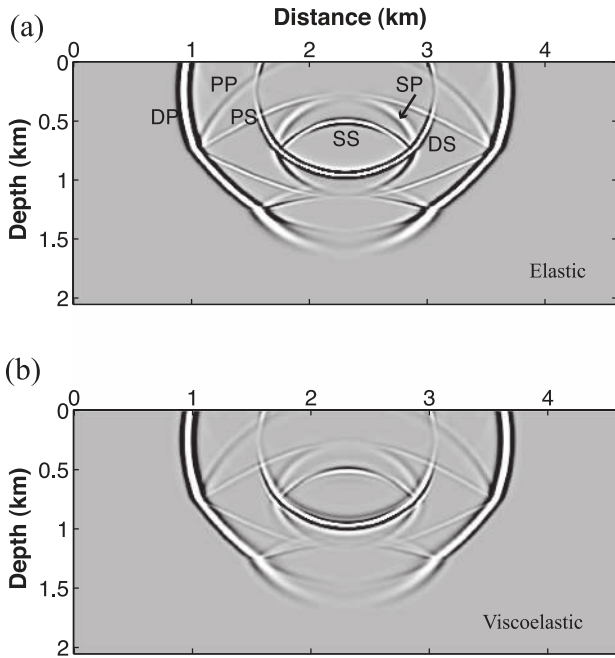

Figure 6. Snapshots of the wavefield (vertical particle velocity) at 0.5 s corresponding to the three-layer model: (a) elastic case and (b) viscoelastic case. The symbols denote: DP: direct *P* wave; DS: direct *S* wave; PP: reflected *P* waves at the first interface; PS: converted *S* waves from *P* waves at the first interface; SS: reflected *S* waves; SP: converted *P* waves from *S* waves at the first interface.

PS waves, the reflected *SP* and *SS* waves and the transmitted *P* and *PS* waves. Figs 7(a) and (b) display the corresponding synthetic seismograms. Fig. 7(c) shows the seismogram computed by the standard linear solid model approach (Zhu *et al.* 2013). As expected, major features, including first arrivals, refractions, reflections, diffractions and multiples, are weaker in the viscoelastic case. Fig. 8 compares traces computed with the present approach with those computed with the viscoelastic modelling approach using a single standard linear solid element. Overall, the amplitudes are comparable.

In the last example, we apply the present approach to the Marmousi model (Fig. 9), which describes strongly heterogeneous media. We assume an *S*-wave velocity $C_s = C_p/1.73$. The low Q_P's
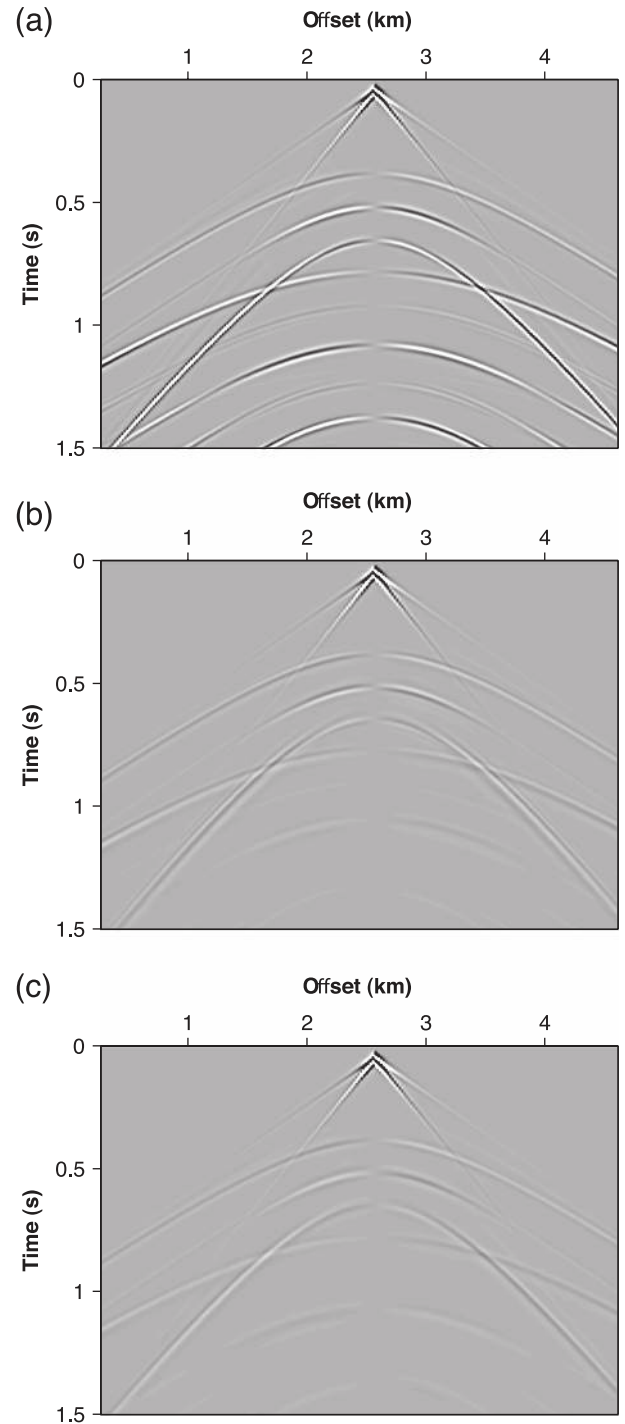

Figure 7. Seismograms (horizontal particle velocity) corresponding to the three-layer model using (a) infinite Q_P and Q_S and (b) the values indicated in Fig. 6. For comparison, using the same attenuation models, we simulated the viscoelastic data (c) by using the standard linear solid model approach.

of the upper part simulate a high-attenuation gas cloudy area in Fig. 9(c). Moreover, we assume $Q_S = Q_P/1.2$. The medium is discretized with 921×481 grid points and uniform vertical and horizontal grid spacings of 6.25 m. Again, PML absorbing strips of width 20 grid points are implemented at the four boundaries of the computational mesh to avoid wraparound. The source denoted by a
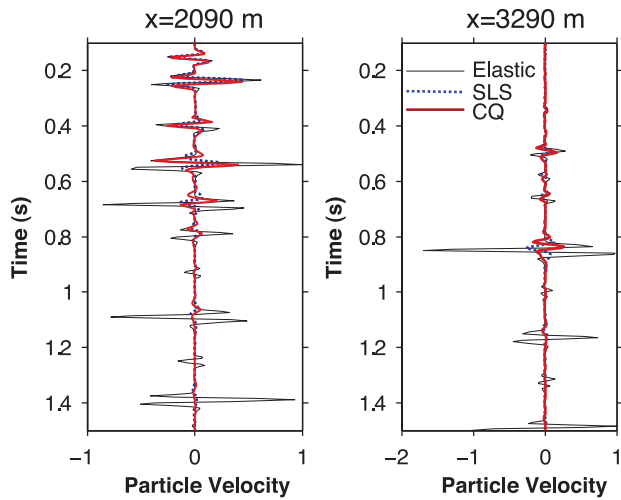
Figure 8. Comparison of corresponding traces of Fig. 7 at horizontal distance 2090 and 3290 m. The black line shows the elastic trace, the blue line shows the viscoelastic case computed with the standard linear solid approach, and the red line shows the viscoelastic case computed with the present approach.

Figure 9. Marmousi *P*-wave velocity (a), density (b), and Q_P (c) models with the properties used in the calculation of the synthetic data. We calculated *S*-wave velocity by $C_s = C_p/1.73$. Also, we calculated $Q_S = Q_P/1.2$. The white star in (a) represents the source at (2881.3, 281.2) m. The receivers are located at a depth of 218.8 m and range from 62.5 to 5687.5 m.

white star in Fig. 9(a) is a vertical force with a Ricker-wavelet time history and a central frequency of 15 Hz, located at (2881, 281) m. The receivers are located at a depth of 219 m and range from 62 to 5687 m, with a spacing 12.5 m. The time step of the modelling algorithm is 0.4 ms. The time length of the simulation is 3 s.

Figs 10(a) and (b) show snapshots of elastic wavefields corresponding to the horizontal and vertical components at 0.9 s, respectively, and Figs 10(c) and (d) show the snapshots in the viscoelastic case. It can be found that the wavefield passing through the high-attenuation gas cloudy zones is attenuated. The wave types (e.g. major reflections) are identifiable. Further, Figs 11(a) and (b) display the corresponding horizontal and vertical particle-velocity synthetic seismograms. This example shows that the proposed fractional viscoelastic wave equation can be used for modelling seismic wave in complex geological models of interest in seismology and exploration geophysics.

4 CONCLUSIONS

We have presented a new formulation for simulating wave propagation in viscoelastic media that avoids the use of memory variables or storing the past wavefields. The method is based on fractional spatial derivatives that are computed with a generalization of the Fourier pseudospectral method to the fractional case. The formulation consists of two sets of fractional Laplacian operators to describe the attenuation of the *P*- and *S*-waves. Setting the respective quality factors to infinite gives the classical elastic formulation. Because the Laplacian operators are evaluated in the spatial domain, the proposed viscoelastic equation is highly efficient, since it avoids the use of additional arrays to store the past values of the wavefields. Since the algorithm is a direct grid method, it holds for all frequencies and arbitrary heterogeneous models.
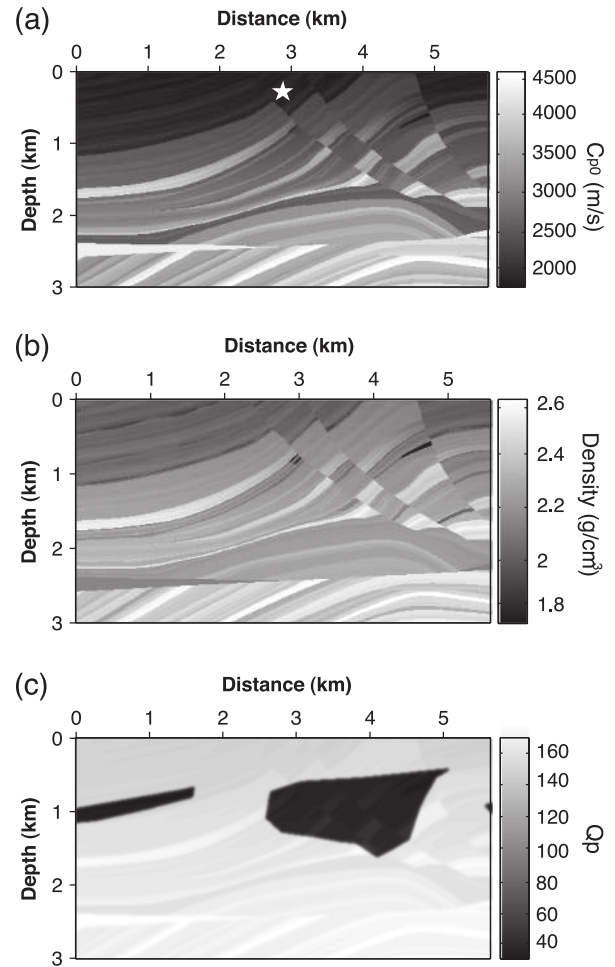
Numerical results of the proposed wave equation for Pierre Shale exhibit the desired constant-*Q* attenuation and dispersion behaviour. Furthermore, comparison to the analytical solution in homogeneous media shows that the algorithm can accurately simulate seismic wave propagation in viscoelastic media. Simulations in inhomogeneous media illustrate the versatility of the methodology.
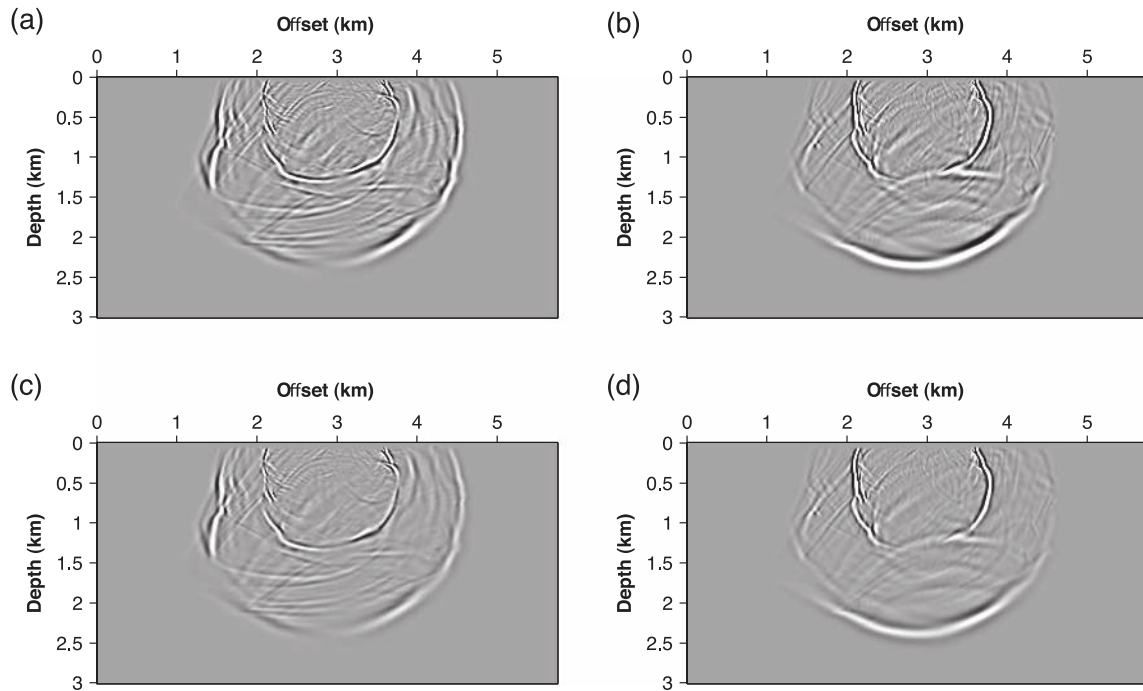
ACKNOWLEDGEMENTS

Figure 10. Wavefield snapshots at 0.9 s. Top: elastic horizontal (a) and vertical (b) particle velocity components. Bottom: viscoelastic horizontal (c) and vertical (d) particle velocity components. Comparing these results, the wave energy (bottom) passing through the high attenuation gas cloudy areas is attenuated.
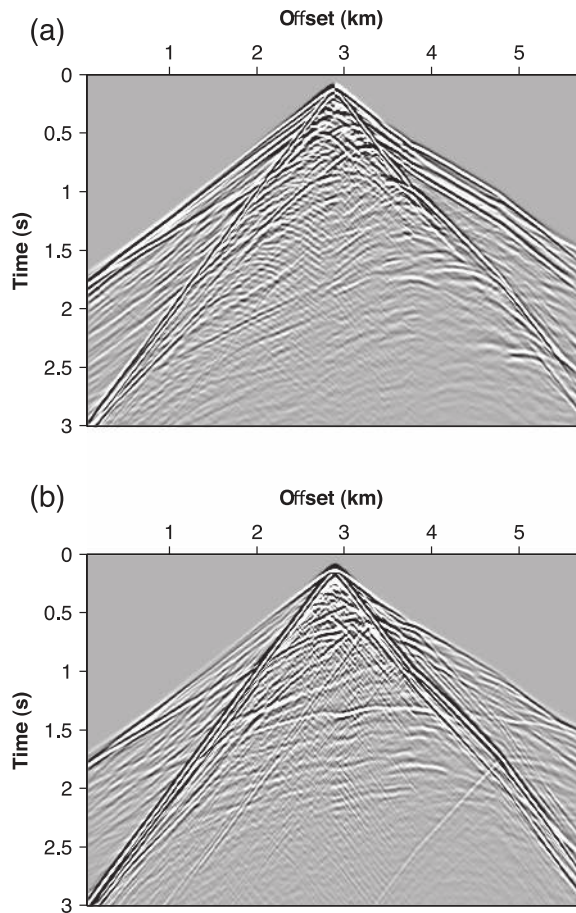

Figure 11. Viscoelastic horizontal (a) and vertical (b) particle-velocity seismograms.

REFERENCES

Berenger, J.P., 1994. A perfectly matched layer for the absorption of electromagnetic waves, *J. Comput. Phys.,* **114,** 185–200.

Bland, D.R., 1960. *The Theory of Linear Viscoelasticity,* Pergamon.

Caputo, M., 1967. Linear model of dissipation whose Q is almost frequency independent-II, *Geophys. J. R. Astron. Soc.,* **13,** 529–539.

Carcione, J.M., 1990. Wave propagation in anisotropic linear viscoelastic media: theory and simulated wavefields, *Geophys. J. Int.,* **101,** 739–750. Erratum: 1992, **111,** 191.

Carcione, J.M., 1999. Staggered mesh for the anisotropic and viscoelastic wave equation, *Geophysics,* **64,** 1863–1866.

Carcione, J.M., 2007. *Wave Fields in Real Media: Theory and Numerical Simulation of Wave Propagation in Anisotropic, Anelastic, Porous and Electromagnetic Media,* Elsevier.

Carcione, J.M., 2009. Theory and modeling of constant-Q P- and S-waves using fractional time derivatives, *Geophysics,* **74**(1), T1–11.

Carcione, J.M., 2010. A generalization of the Fourier pseudospectral method, *Geophysics,* **75**(6), A53–A56.

Carcione, J.M. & Kosloff, D., 2013. Representation of matched-layer kernels with viscoelastic mechanical models, *Int. J. Numer. Anal. Mod.,* **10,** 221–232.

Carcione, J.M., Helbig, K. & Helle, H.B., 2003. Effects of pressure and saturating fluid on wave velocity and attenuation of anisotropic rocks, *Int. J. Rock Mech. Min. Sci.,* **40,** 389–403.

Carcione, J.M., Kosloff, D. & Kosloff, R. 1988. Wave propagation in a linear viscoelastic medium, *Geophys. J. R. Astron. Soc.,* **95,** 597–611.

Carcione, J.M., Cavallini, F., Mainardi, F. & Hanyga, A., 2002. Time-domain seismic modeling of constant-Q wave propagation using fractional derivatives, *Pure appl. Geophys.,* **159,** 1719–1736.

Caputo, M. & Mainardi, F., 1971. A new dissipation model based on memory mechanism, *Pure appl. Geophys.,* **91,** 134–147.

Chen, W. & Holm, S., 2004. Fractional Laplacian time-space models for linear and nonlinear lossy media exhibiting arbitrary frequency power-law dependency, *J. acoust. Soc. Am.,* **115,** 1424–1430.

Dvorkin, J.P. & Mavko, G., 2006. Modeling attenuation in reservoir and nonreservior rock, *Leading Edge* **25,** 194–197.

Eason, J., Fulton, J. & Sneddon, I.N., 1956. The generation of waves in an infinite elastic solid by variable body forces, *Phil. Trans. R. Soc. London,* **A248,** 575–607.

Hestholm, S.O., 1999. 3-D finite difference viscoelastic wave modelling including surface topography, *Geophys. J. Int.,* **139,** 852–878.

Komatitsch, D., Liu, Q., Tromp, J., Suss, P., Stidham, C. & Shaw, J.H., 2004. Simulations of ground motion in the Los Angeles basin based upon the spectral-element method, *Bull. seism. Soc. Am.,* **94**(1), 187–206.

Kjartansson, E., 1979. Constant-*Q* wave propagation and attenuation, *J. geophys. Res.,* **84,** 4737–4748.

Özdenvar, T. & McMechan, G.A., 1996. Causes and reduction of numerical artifacts in pseudo-spectral wavefield extrapolation, *Geophys. J. Int.,* **126,** 819–828.

McDonal, F.J., Angona, F.A., Mills, R.L., Sengbush, R.L., Van Nostrand, R.G. & White, J.E., 1958. Attenuation of shear and compressional waves in Pierre shale, *Geophysics,* **23,** 421–439.

Picotti, S. & Carcione, J.M., 2006. Estimating seismic attenuation (Q) in the presence of random noise, *J. Seism. Explor.,* **15,** 165–181.

Podlubny, I., 1999. *Fractional Differential Equations,* Academic Press, ISBN 0125588402.

Robertsson, J.O., Blanch, J.O. & Symes, W.W., 1994. Viscoelastic finite-difference modeling, *Geophysics,* **59,** 1444–1456.

Treeby, B.E. & Cox, B.T., 2010. Modeling power law absorption and dispersion for acoustic propagation using the fractional Laplacian, *J. acoust. Soc. Am.,* **127,** 2741–2748.

Xu, T. & McMechan, G.A., 1995. Composite memory variables for viscoelastic synthetic seismograms, *Geophys. J. Int.,* **121,** 634–639.

Wuenschel, P.C., 1965. Dispersive body waves - an experimental study, *Geophysics,* **30,** 539–551.

Zhu, T., Carcione, J.M. & Harris, J.M., 2013. Approximating constant-*Q* seismic propagation in the time domain, *Geophys. Prospect.,* **61**(5), 931–940.

Zhu, T. & Harris, J.M., 2013. Modeling acoustic wave propagation in heterogeneous attenuating media using decoupled fractional Laplacians, *Geophysics,* in revision.

APPENDIX A: CONSTANT-*Q* PHASE VELOCITY AND ATTENUATION

Let us assume a plane-wave kernel of the form $\exp(i\omega t - i\mathbf{k}\cdot\mathbf{r})$, where the wavenumber vector $\mathbf{k}$ is complex-valued. Then, eq. (5) yields the following complex modulus

$$M = M_0 \left(\frac{c_0 k}{\omega_0}\right)^{2\gamma} \left[\cos(\pi\gamma) + \frac{i\omega\sin(\pi\gamma)}{c_0 k}\right]. \tag{A1}$$

It can be shown that for realistic Q values we can use the relation $c_0 k = \omega$ and after some calculations the complex velocity obtained from eq. (A1) is given by

$$\upsilon_c = \frac{\omega}{k} = \sqrt{\frac{M}{\rho}}, \text{ where } M = M_0 \left(\frac{i\omega}{\omega_0}\right)^{2\gamma}, \tag{A2}$$

where M is the complex modulus. The phase velocity is

$$\upsilon_{ph} = \mathrm{Re}^{-1}(\upsilon_c^{-1}) = \sqrt{\frac{M_0}{\rho}} \left(\frac{\omega}{\omega_0}\right)^{\gamma} \Big/ \cos\left(\frac{\pi\gamma}{2}\right) = c_0 \left(\frac{\omega}{\omega_0}\right)^{\gamma} \tag{A3}$$

and the quality factor is

$$Q = \frac{\mathrm{Re}(M)}{\mathrm{Im}(M)} = \cot(\pi\gamma) \tag{A4}$$

(Carcione, 2007). These equations are identical to those of the constant-*Q* model (Kjartansson 1979; Carcione *et al.* 2002) and can be used for *Q* values as low as five.

Similarly, the complex velocities corresponding to the viscoelastic case are given by

$$\upsilon_P = \sqrt{\frac{M(\omega)}{\rho}} \quad\text{and}\quad \upsilon_S = \sqrt{\frac{\mu(\omega)}{\rho}}, \tag{A5}$$

where

$$M(\omega) = M_0 \left(\frac{i\omega}{\omega_0}\right)^{2\gamma_P} \quad\text{and}\quad \mu(\omega) = \mu_0 \left(\frac{i\omega}{\omega_0}\right)^{2\gamma_S}, \tag{A6}$$

while the phase velocities are

$$c_{phP}(\omega) = c_{P0} \left(\frac{\omega}{\omega_0}\right)^{\gamma_P} \quad\text{and}\quad c_{phS}(\omega) = c_{S0} \left(\frac{\omega}{\omega_0}\right)^{\gamma_S}. \tag{A7}$$

The spatial quality factors are

$$Q_P = \frac{\mathrm{Re}(M)}{\mathrm{Im}(M)} = \cot(\pi\gamma_P) \tag{A8}$$

and

$$Q_S = \frac{\mathrm{Re}(\mu)}{\mathrm{Im}(\mu)} = \cot(\pi\gamma_S). \tag{A9}$$

These equations, already given in Carcione (2009), can be used for realistic *Q* values to estimate the seismic attenuation and phase velocity, otherwise, for very low *Q* values, their calculation requires the solution of an implicit equation on the complex velocities.

APPENDIX B: 2-D VISCOELASTIC WAVE EQUATION IN THE TIME DOMAIN

The 2-D velocity-stress formulation of the wave equation combines eqs (16), (21) and (22) with the equations of momentum conservation (Carcione 2007). We obtain

$$\rho\partial_t \upsilon_1 = (\partial_1 \sigma_{11} + \partial_3 \sigma_{13} + f_1), \tag{B1}$$

$$\rho\partial_t \upsilon_3 = (\partial_1 \sigma_{13} + \partial_3 \sigma_{33} + f_3), \tag{B2}$$

$$\sigma_{11} = \tau_P A_P \frac{\partial}{\partial t}(\varepsilon_{11} + \varepsilon_{33}) + \eta_p B_P(\varepsilon_{11} + \varepsilon_{33})$$
$$- 2\tau_S A_S \frac{\partial}{\partial t}\varepsilon_{33} - 2\eta_S B_S \varepsilon_{33}, \tag{B3}$$

$$\sigma_{33} = \tau_P A_P \frac{\partial}{\partial t}(\varepsilon_{11} + \varepsilon_{33}) + \eta_p B_P(\varepsilon_{11} + \varepsilon_{33})$$
$$- 2\tau_S A_S \frac{\partial}{\partial t}\varepsilon_{11} - 2\eta_S B_S \varepsilon_{11}, \tag{B4}$$

$$\sigma_{13} = 2\tau_S A_S \frac{\partial}{\partial t}\varepsilon_{13} + 2\eta_S B_S \varepsilon_{13}, \tag{B5}$$

$$\partial_t \varepsilon_{11} = \partial_1 \upsilon_1, \tag{B6}$$

$$\partial_t \varepsilon_{33} = \partial_3 \upsilon_3, \tag{B7}$$

$$\partial_t \varepsilon_{13} = \frac{1}{2}(\partial_1 \upsilon_3 + \partial_3 \upsilon_1), \tag{B8}$$

where υ_i, ε_{ij} and f_i denote particle velocity, strain and body force components, respectively, and

$$A_{P,S} = \left(-\nabla^2\right)^{\gamma_{P,S}-1/2}, \quad B_{P,S} = \left(-\nabla^2\right)^{\gamma_{P,S}}. \tag{B9}$$

APPENDIX C: ANALYTIC SOLUTION IN HOMOGENEOUS VISCOELASTIC MEDIA

The solution of the wavefield generated by an impulsive point force in a 2-D elastic medium has been given by Eason *et al.* (1956) (see Carcione 2007). For a force acting in the positive z-direction, the displacement solutions can be expressed as

$$u_1(r, t) = \left(\frac{F_0}{2\pi\rho}\right) \frac{xz}{r^2} [G_1(r, t) + G_3(r, t)], \tag{C1}$$

$$u_3(r, t) = \left(\frac{F_0}{2\pi\rho}\right) \frac{1}{r^2} [z^2 G_1(r, t) - x^2 G_3(r, t)], \tag{C2}$$

where F_0 is a constant that gives the magnitude of the force, $r^2 = x^2 + z^2$,

$$G_1(r, t) = \frac{1}{c_P^2}(t^2 - \tau_P^2)^{-1/2} H(t - \tau_P) + \frac{1}{r^2}(t^2 - \tau_P^2)^{1/2} H(t - \tau_P)$$
$$- \frac{1}{r^2}(t^2 - \tau_S^2)^{1/2} H(t - \tau_S), \tag{C3}$$

$$G_3(r, t) = -\frac{1}{c_S^2}(t^2 - \tau_S^2)^{-1/2} H(t - \tau_S) + \frac{1}{r^2}(t^2 - \tau_P^2)^{1/2} H(t - \tau_P)$$
$$- \frac{1}{r^2}(t^2 - \tau_S^2)^{1/2} H(t - \tau_S), \tag{C4}$$

$$\tau_P = \frac{r}{c_P}, \ \tau_S = \frac{r}{c_S}, \tag{C5}$$

c_P and c_S are the compressional and shear wave phase velocities and H is the Heaviside function. To apply the correspondence principle and obtain the anelastic solution, one needs the elastic frequency domain solution (Bland 1960; Carcione *et al.* 1988; Carcione 2007). Using the transform pairs of the zero- and first-order Hankel functions of the second kind,

$$\int_{-\infty}^{\infty} \frac{1}{\tau^2}(t^2 - \tau^2)^{1/2} H(t - \tau) \exp(i\omega t)dt = \frac{i\pi}{2\omega\tau} H_1^{(2)}(\omega\tau), \tag{C6}$$

$$\int_{-\infty}^{\infty} \frac{1}{\tau^2}(t^2 - \tau^2)^{-1/2} H(t - \tau) \exp(i\omega t)dt = -\frac{i\pi}{2} H_0^{(2)}(\omega\tau), \tag{C7}$$

we obtain

$$u_1(r, \omega, c_p, c_s) = \left(\frac{F_0}{2\pi\rho}\right) \frac{xz}{r^2} [\tilde{G}_1(r, \omega, c_p, c_s) + \tilde{G}_3(r, \omega, c_p, c_s)], \tag{C8}$$

$$u_3(r, \omega, c_p, c_s) = \left(\frac{F_0}{2\pi\rho}\right) \frac{1}{r^2} [z^2 \tilde{G}_1(r, \omega, c_p, c_s) - x^2 \tilde{G}_3(r, \omega, c_p, c_s)], \tag{C9}$$

where

$$\tilde{G}_1(r, \omega, c_p, c_s) = -\frac{i\pi}{2} \left[\frac{1}{c_p^2} H_0^{(2)}\left(\frac{\omega r}{c_p}\right) + \frac{1}{\omega r c_s} H_1^{(2)}\left(\frac{\omega r}{c_s}\right) - \frac{1}{\omega r c_p} H_1^{(2)}\left(\frac{\omega r}{c_p}\right) \right], \tag{C10}$$

and

$$\tilde{G}_3(r, \omega, c_p, c_s) = \frac{i\pi}{2} \left[\frac{1}{c_s^2} H_0^{(2)}\left(\frac{\omega r}{c_s}\right) - \frac{1}{\omega r c_s} H_1^{(2)}\left(\frac{\omega r}{c_s}\right) + \frac{1}{\omega r c_p} H_1^{(2)}\left(\frac{\omega r}{c_p}\right) \right], \tag{C11}$$

The complex wave velocities given in Appendix B are used to replace the real-valued velocities in the equations above. Then, the 2-D viscoelastic Green's function can be expressed as

$$u_{1,3}(r, \omega) = \begin{cases} u_{1,3}(r, \omega, V_P, V_S), & \omega \geq 0, \\ u_{1,3}^*(r, -\omega, V_P, V_S), & \omega < 0, \end{cases} \tag{C12}$$

where the asterisk denotes complex conjugate. This frequency domain form ensures that the solution is real in the time domain. Multiplication with the source time function and a numerical inversion by the discrete Fourier transform yield the desired time-domain displacement solution ($\tilde{G}_3$ and $\tilde{G}_3$ assumed to be zeros at $\omega = 0$ because the Hankel functions are singular). The particle-velocity solutions are the time derivative of the displacement solutions.